Chirality, magnetic charge and other strange entities in resonant x-ray Bragg diffraction

2009 J. Phys.: Condens. Matter 21 474214

(http://iopscience.iop.org/0953-8984/21/47/474214)

IOP PUBLISHING JOURNAL OF PHYSICS: CONDENSED MATTER

J. Phys.: Condens. Matter **21** (2009) 474214 (11pp) doi:10.1088/0953-8984/21/47/474214

Chirality, magnetic charge and other strange entities in resonant x-ray Bragg diffraction

Stephen W Lovesey[1,2] **and Valerio Scagnoli**[3]

[1] ISIS Facility, Harwell Science and Innovation Campus, Oxfordshire OX11 0QX, UK
[2] Diamond Light Source Ltd, Oxfordshire OX11 0DE, UK
[3] European Synchrotron Radiation Facility, F-38043 Grenoble Cedex 9, France

Received 7 April 2009, in final form 21 July 2009
Published 5 November 2009
Online at stacks.iop.org/JPhysCM/21/474214

Abstract
Subtleties in the electronic structure of complex materials can be directly observed, in great detail, by means of the Bragg diffraction of x-rays whose energy matches an atomic resonance. Strange atomic multipoles can be encountered in the interpretation of measured Bragg intensities, e.g., chirality and magnetic charge. Additionally, the x-ray technique allows the direct observation of the enantiomorphic screw-axis in chiral crystals, such as tellurium, low quartz and berlinite.

(Some figures in this article are in colour only in the electronic version)

1. Introduction

Up to a certain point it is useful to describe the motif of magnetic moments in a crystal by a cartoon in which vectors, representing dipole moments, are placed at sites occupied by magnetic ions. For many magnetic materials such a cartoon conveys but a small fraction of essential information about the distribution of charge and magnetism that depend on angular anisotropy in unfilled electron states. In general, therefore, a family of multipoles, consisting of monopoles, dipoles, quadrupoles, etc, is required for a comprehensive representation of electron degrees of freedom.

Resonant x-ray Bragg diffraction exposes multipoles in a crystal with directness of purpose not available with any other experimental method in the science of materials. Seminal observations of this diffraction came from Templeton and Templeton [1] and Finkelstein *et al* [2], with timely theoretical analyses by Dmitrienko [3] and Carra and Thole [4]. In 2005, Dmitrienko *et al* [5] surveyed experiments on non-magnetic materials utilizing resonant diffraction. At about the same time, Lovesey *et al* [6] and Collins *et al* [7] shaped theoretical concepts in resonant x-ray diffraction and absorption by both non-magnetic and magnetic materials. Coexistence of spontaneous order in the charge and the magnetic degrees of freedom of electrons is a multiferroic modification of properties of intense current interest in materials science [8–12]. There are counterintuitive atomic properties whose existence summons in to play strange electron variables. These are not ornaments in an ephemeral theory but entities significant to an atomic theory of electron properties and, also, directly observed in x-ray diffraction [6, 7].

We endeavour in this article to gather, necessarily in succinct form, principal concepts and tools currently employed in the analysis of observations made on electrons in crystals with the resonant diffraction of x-rays. Firmly established concepts and tools are illustrated in a survey of published data gathered on a few materials of particular current interest in the science of materials. Additionally, we strive to convey emerging science; discoveries about electronic properties of complex materials and concepts they beget now develop extremely rapidly. In sections 3, 4.3, appendices A and B we report results that have not previously been published. To help avoid in the paper too much of a confused medley of observations, ideas and technical stuff appendix C contains comments on some of it. Thus we move ahead in the certain knowledge that the reader has at hand a summary of definitions and technical stuff essential to our exposition.

If the site in the crystal used by the resonant ion is a centre of inversion symmetry parity-odd multipoles are forbidden. Allowed, parity-even multipoles possess a one-to-one correspondence between rank, K, and sign with respect to time-reversal, namely, time-odd (time-even) multipoles have odd (even) rank. Also, parity-even multipoles with even K originate from true-tensors, and multipoles with odd K originate from pseudo-tensors. In particular, the parity-even

Table 1. Shown are cameo composite operators of rank $K = 0$ (scalar or monopole), 1 (dipole) and 2 (quadrupole) which can be used to represent time-odd (magneto-electric; $\mathbf{G}_K$) and time-even (polar; $\mathbf{U}_K$) multipoles that arise in the E1–M1, parity-odd resonant event. See appendix C for additional information. Basic operators are; $\mathbf{R}$ position (polar vector), $\boldsymbol{\mu}$ magnetic moment $= \mathrm{L} + 2\mathrm{S}$ (axial vector), and $\boldsymbol{\Omega} = (\boldsymbol{\mu} \times \mathbf{R} - \mathbf{R} \times \boldsymbol{\mu})$ anapole operator. Electric and magnetic dipole operators, E1 and M1, can be represented by $\mathbf{R}$ and $\boldsymbol{\mu}$, respectively. Composite operators with even-rank are pseudo-tensors, and tensors of odd-rank are true-tensors. It can be shown that $\boldsymbol{\mu} \cdot \mathbf{R} = 2\mathbf{S} \cdot \mathbf{R}$ and $\boldsymbol{\mu} \cdot \boldsymbol{\Omega} = 4i\mathbf{S} \cdot \mathbf{R}$. Mean values of the magneto-electric and polar monopoles are magnetic charge and chirality, or helicity, respectively, which are pseudo-scalars. For comparison, operators $\mathbf{T}_K$ suitable for the E1–E1, parity-even resonant event are included. With $K = 2$ the symbol $\otimes$ denotes a tensor product.

Tensor rank K	0	1	2
Magneto-electric; $\mathbf{G}_K$	$\boldsymbol{\mu} \cdot \mathbf{R}$	$\boldsymbol{\Omega}$	$\{\boldsymbol{\mu} \otimes \mathbf{R}\}^2$
Polar; $\mathbf{U}_K$	$\boldsymbol{\mu} \cdot \boldsymbol{\Omega}$	$\mathbf{R}$	$\{\boldsymbol{\Omega} \otimes \boldsymbol{\mu}\}^2$
Parity-even; $\mathbf{T}_K$	1	$\boldsymbol{\mu}$	$\{\boldsymbol{\mu} \otimes \boldsymbol{\mu}\}^2$

multipole with $K = 1$ is a time-odd pseudo-vector (axial vector) proportional to the magnetic moment associated with the ion as in table 1.

When the centre of inversion symmetry is absent, parity-odd multipoles can be different from zero and such multipoles with even K are pseudo-tensors and those with odd K are true-tensors. Parity-odd, time-even multipoles $\langle \mathbf{U}_K \rangle$ are called polar. (Angular brackets denote the expectation value of the enclosed quantum-mechanical operator.) Polar multipoles with rank 0 and 1 have an immediate physical significance, for chirality $\equiv \langle \mathbf{U}_0 \rangle$ and displacement $\equiv \langle \mathbf{U}_1 \rangle$. Parity-odd, time-odd multipoles $\langle \mathbf{G}_K \rangle$ are called magneto-electric by analogy with a necessary condition for the magneto-electric effect that the inversion is accompanied by time-reversal. The magneto-electric monopole, $\langle \mathbf{G}_0 \rangle$, is a magnetic charge [13, 14] while the dipole, $\langle \mathbf{G}_1 \rangle$, is an anapole, or toroidal moment. Table 1 lists composite quantum-mechanical operators that can be used as cameos of parity-odd and parity-even multipoles.

The nature of the resonant event determines many attributes of multipoles contributing to the measured Bragg intensity. In keeping with standard practice in absorption spectroscopy, absorption via the electron dipole and magnetic dipole are labelled E1 and M1 (electric and magnetic dipole operators are represented by polar ($\mathbf{R}$) and axial ($\boldsymbol{\mu}$) vectors, respectively, cf table 1). However, scattering is a two-stage process and E1–E1 is the strongest process, unless forbidden by selection rules. Many factors contribute to selection rules in Bragg diffraction, which itself can only occur when a strict geometric rule, involving the spacing of ions in a crystal and the wavelength of illuminating radiation, is met (Bragg's law). Since E1 has a definite parity the E1–E1 event is parity-even and it can only reveal electron properties with the same condition. Electric and magnetic dipole moments have opposite parities. Thus the E1–M1 event is parity-odd and capable of revealing atomic polar and magneto-electric multipoles.

Engaging an atomic resonance in diffraction has other benefits. The atom type is labelled and the Bragg intensity enhanced, making visible very small contributions, currently at the level of one part in 10^8, which would otherwise go undetected. Polarization analysis yields even more valuable information because scattering channels with rotated polarization, forbidden in Thomson scattering, can be different from zero. In fact, chirality and magnetic charge reside in rotated polarization channels (appendix B). Additionally, intensities of space group forbidden, or weak, reflections provide information not available from the real and imaginary parts of the refractive index, namely, birefringent dispersion and dichroism. Magnetic charge is not observed in dichroism while chirality contributes to natural circular dichroism [6, 7].

Being parity-odd the E1 photo-electric event connects atomic states with opposite parity. Direct observation of multipoles possessed by d-like valence electrons, by resonant Bragg diffraction, therefore demands absorption to occur at an intermediate state that is p-like, which is called an L-state, or L-edge. E1 absorption at an intermediate state which is s-like, and called the K-edge, gives access to p-like valence states at the absorption site that contain second-hand information of minimal value on d-like multipoles.

In the following section, we summarize theoretical results for a resonant scattering amplitude suitable for analysis of Bragg diffraction and dichroism. Thereafter, in section 3, we discuss the unit-cell structure factor with particular attention to the E1–M1 resonant event, which has recently become a subject of renewed interest. Our work is based on an atomic model of the magnetic material, which has a long and distinguished history in the theory of magnetism. In general, scattering is enhanced by parity-even (E1–E1, E2–E2) and parity-odd (E1–M1, E1–E2) resonant events and our amplitudes respect global symmetries inherent from quantum-electrodynamics. Comprehensive statements for Bragg diffraction with rotation of the crystal (azimuthal-angle scan) and E1–E1, E1–E2, and E2–E2 enhancements have recently been published by us [15] and here we complement this body of work with corresponding statements for Bragg diffraction enhanced by an E1–M1 event. In section 4 we survey a few recent and representative experiments. A discussion is given in section 5.

2. Resonant scattering amplitude

The scattering amplitude on which we base our work is calculated from quantum-electrodynamics [6, 7, 16]. In the derivation, the QED amplitude, or scattering matrix, is developed in the small quantity E/mc^2 where E is the primary photon energy and $mc^2 = 0.511$ MeV. At the second level of smallness in this quantity the amplitude contains resonant processes that may dominate all other contributions to the amplitude should E match an atomic resonance with an energy Δ. Assuming also that virtual intermediate states are spherically symmetric [17–21], to a good approximation, the scattering amplitude in the region of a resonance is of the form,

$$f \approx F_{\mu'\nu}/(E - \Delta + \mathrm{i}\Gamma/2) = G_{\mu'\nu}, \qquad (2.1)$$

where Γ is the total width of the resonance. In (2.1), $F_{\mu'\nu}$ is a unit-cell structure factor for Bragg diffraction in the scattering channel with primary (secondary) polarization ν (μ'). We use

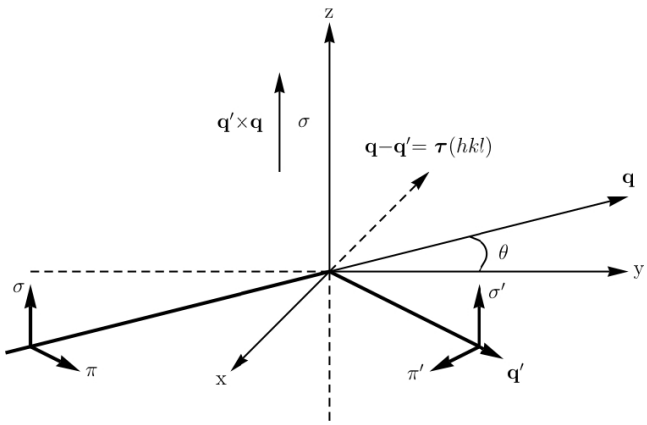

Figure 1. Shown is the Cartesian coordinate system (x, y, z) adopted for Bragg diffraction and the relation to states of polarization, labelled σ and π, in the primary (unprimed) and secondary (primed) beams of photons.

the standard convention of labelling these polarization states (figure 1), in which σ-polarization is normal to the plane of scattering and π-polarization is parallel to the plane.

The unit-cell structure factor, $F_{\mu'\nu}$, contains $\langle \hat{J}_{\mu'}(-\mathbf{q}')\, \hat{J}_{\nu}(\mathbf{q})\rangle$ where $\hat{J}_{\nu}(\mathbf{q})$ is the current operator for electrons and a primary (secondary) photon wavevector $\mathbf{q}(\mathbf{q}')$. The expectation value of the product of current operators is performed with the equilibrium, electron ground-state wavefunction. Evaluated with $\mathbf{q} = \mathbf{q}' = 0$ structure factors describes diffraction with enhancement by E1 events. The first correction to the current of electrons, in an expansion in terms of the wavevector, introduces additional resonant contributions E1–M1, E1–E2, E2–E2, etc.

The presence of spin, **S**, in the M1 operator allows enhancement at a K-edge which would otherwise be forbidden on account of zero orbital angular momentum, **L**. To engage the M1 event in diffraction, or dichroism, valence and intermediate states have common angular momentum, because matrix elements of **L** and **S** are diagonal with respect to orbital angular momentum. Thus absorption at a K-edge can engage M1 when s-like valence states are available. In addition, intermediate and valence states must not be orthogonal. Like the other parity-odd event we discuss, E1–E2, the E1–M1 event is allowed when valence states at the site of the resonant ion are an admixture of orbitals with different parities, which can occur when the site is not a centre of inversion symmetry. This requirement on the resonant site for non-zero contributions to Bragg diffraction from parity-odd events does not mean that the crystal structure must be non-centrosymmetric.

Appendix A explores properties of parity-odd multipoles using a specific model wavefunction by way of further orientation to multipoles appearing in diffraction enhanced by an E1–M1 event.

3. Unit-cell structure factor

The generic form of a unit-cell structure factor is,

$$F_{\mu'\nu} = \sum_{K} \mathbf{J}^{K}_{\mu'\nu} \cdot \mathbf{D}^{K} \cdot \mathbf{\Psi}^{K}, \tag{3.1}$$

where the spherical tensor $\mathbf{J}^{K}_{\mu'\nu}$ describes the condition of the primary and secondary photons, and there is a different $\mathbf{J}^{K}_{\mu'\nu}$ for each resonant event. The quantity $\mathbf{D}^{K}$ in (3.1) is a rotation matrix employed to orientate the crystal in right-handed Cartesian coordinates (x, y, z) that describe the scattering geometry (figure 1). We choose σ-polarization parallel to the z-axis, and the Bragg wavevector $(\mathbf{q} - \mathbf{q}')$ anti-parallel to the x-axis. The rotation matrix is a function of the azimuthal angle, ψ, that measures rotation of the crystal about the Bragg wavevector. Lastly in (3.1), $\mathbf{\Psi}^{K}$ is a structure factor of the form,

$$\mathbf{\Psi}^{K} = \sum_{d} \langle \mathbf{O}_{K} \rangle_{d} \exp\{\mathrm{i}\mathbf{d} \cdot (\mathbf{q} - \mathbf{q}')\}, \tag{3.2}$$

where the sum is over all resonant ions in a unit cell of the crystal. The Bragg condition for diffraction is met when the wavevector $(\mathbf{q} - \mathbf{q}')$ coincides with a vector in the reciprocal lattice for the crystal structure, $\tau(hkl)$. Equation (3.2) is written in terms of multipoles $\langle \mathbf{O}_{K} \rangle$ that might be parity-even, denoted by $\langle \mathbf{T}_{K} \rangle$, or parity-odd, namely, $\langle \mathbf{U}_{K} \rangle$ or $\langle \mathbf{G}_{K} \rangle$.

Expressions for $\mathbf{J}^{K}_{\mu'\nu}$ appropriate for E1–E1, E1–E2 and E2–E2 events have been given in previous publications. Universal forms of $F_{\mu'\nu}$ as a function of the azimuthal angle are given in [15]. Here we follow on with the corresponding information for E1–M1 [6, 7].

To this end, write $\mathbf{D}^{K}$ as a product of two rotations, one to orientate the crystal to the setting $\psi = 0$ in coordinates (x, y, z), and one to rotate the crystal from this setting about the Bragg wavevector. Denote by Ξ Euler angles for the first rotation. These angles are a function of the Bragg wavevector. Orthonormal axes in the crystal to which the Bragg wavevector is referred nominally coincide with (x, y, z). Axes of the unit cell of the crystal are convenient for this purpose when they are orthonormal while in the more general case, including monoclinic and hexagonal structures, it is necessary to erect orthonormal principal axes in the crystal that do not coincide with edges of the unit cell. Following [15], we introduce quantities $\mathbf{A}_{K,Q}$ and $\mathbf{B}_{K,Q}$ that are, respectively, even and odd functions of the projection Q, namely,

$$\begin{aligned} \mathbf{A}_{K,Q} + \mathbf{B}_{K,Q} &= \sum_{q} \mathbf{D}^{K}_{Q,q}(\Xi) \mathbf{\Psi}^{K}_{q}, \\ \mathbf{A}_{K,Q} - \mathbf{B}_{K,Q} &= \sum_{q} \mathbf{D}^{K}_{-Q,q}(\Xi) \mathbf{\Psi}^{K}_{q}. \end{aligned} \tag{3.3}$$

By definition $\mathbf{B}_{K,0} = 0$.

In terms of these quantities a unit-cell structure factor is,

$$\mathbf{F}_{\mu'\nu} = \sum_{K} \mathbf{J}^{K}_{\mu'\nu} \cdot \mathbf{D}^{K}(\psi) \cdot (\mathbf{A}_{K} + \mathbf{B}_{K}). \tag{3.4}$$

The sense of rotation about the wavevector is counter clockwise when the wavevector points to the observer, and at the origin of the azimuthal-angle scan $\mathbf{D}^{K}_{Q,q}(0) = \exp\{\mathrm{i}\pi(Q - q)/2\} d^{K}_{Q,q}(0) = \delta_{Q,q}$.

For the E1–M1 event, $\mathbf{J}^{K}_{\mu'\nu}$ is proportional to $\tilde{N}_{K,Q} \pm N_{K,Q}$ and values of these factors are listed in table 2 for all $\mu'\nu$. With

Table 2. Factors listed in the table appear in the unit-cell structure factor (3.5) for Bragg diffraction with enhancement by the E1–M1 resonant event. The angle θ is the Bragg angle with $\mathbf{q}\cdot\mathbf{q}' = q^2\cos(2\theta)$. In figure 1, σ-polarization is normal to the plane of scattering, parallel to the z-axis, and π-polarization is parallel to the plane. $N_{K,-Q} = (-1)^{K+Q}(N_{K,Q})^*$ and $\tilde{N}_{K,Q}$ satisfies the same identity.

	$\tilde{N}_{K,Q} - N_{K,Q}$	$\tilde{N}_{K,Q} + N_{K,Q}$
$(\sigma'\sigma)$		
$K = 1,\ Q = 1$	$-\mathrm{i}\sin(\theta)$	$-\cos(\theta)$
$K = 2,\ Q = 1$	$-\mathrm{i}\sin(\theta)$	$-\cos(\theta)$
$(\pi'\pi)$		
$K = 1,\ Q = 1$	$\mathrm{i}\sin(\theta)$	$-\cos(\theta)$
$K = 2,\ Q = 1$	$-\mathrm{i}\sin(\theta)$	$\cos(\theta)$
$(\pi'\sigma)$		
$K = Q = 0$	$-2\cos^2(\theta)/\sqrt{3}$	$2\sin^2(\theta)/\sqrt{3}$
$K = 1,\ Q = 0$	$-\mathrm{i}\sin(2\theta)/\sqrt{2}$	$-\mathrm{i}\sin(2\theta)/\sqrt{2}$
$K = 2,\ Q = 0$	$\{1 + 2\sin^2(\theta)\}/\sqrt{6}$	$-\{1 + 2\cos^2(\theta)\}/\sqrt{6}$
$K = 2,\ Q = 2$	$1/2$	$1/2$
$(\sigma'\pi)$		
From $(\pi'\theta)$ through sign change and $\theta \Rightarrow -\theta$		From $(\pi'\theta)$ through $\theta \Rightarrow -\theta$

$\psi = 0$, and $K = 0$, 1 and 2,

$$F_{\mu'\nu}(\text{E1–M1}) = \sum_K i^{K-1} \sum_Q (-1)^Q \{-\mathrm{i}[\mathbf{A}_{K,Q} + \mathbf{B}_{K,Q}](g) \times [\tilde{N}_{K,-Q} + N_{K,-Q}] + [\mathbf{A}_{K,Q} + \mathbf{B}_{K,Q}](u) \times [\tilde{N}_{K,-Q} - N_{K,-Q}]\}. \quad (3.5)$$

In this expression, labels g and u are attached to $[\mathbf{A}_{K,Q} + \mathbf{B}_{K,Q}]$ to indicate whether they are made from (3.2) with multipoles $\langle \mathbf{G}_K \rangle$ or $\langle \mathbf{U}_K \rangle$, and the different combinations $\tilde{N}_{K,Q} + N_{K,Q}$ and $\tilde{N}_{K,Q} - N_{K,Q}$ accompany magneto-electric or polar multipoles. Appendix B contains values of $F_{\mu'\nu}$ (E1–M1) as a function of azimuthal angle, and [15] contains corresponding unit-cell structure factors for E1–E1, E1–E2 and E2–E2 resonant events.

By way of examples of structure factors for an E1–M1 event, we record expressions appropriate for gallium ferrate and Bragg reflections $(0, k, 0)$ with odd Miller index k. These reflections are forbidden by the space group and such reflections are often referred to as weak reflections. Using results for Ψ^K_Q for gallium ferrate derived by Lovesey *et al* [22], and expressions for E1–M1 structure factors in appendix B, one quickly finds $F_{\sigma'\sigma}(\text{E1-M1}) = F_{\pi'\pi}(\text{E1-M1}) = 0$. For the channel with rotated polarization we find,

$$F_{\pi'\sigma}(\text{E1–M1}) = -(\mathrm{i}B/\sqrt{2})\sin(2\theta)\cos(\psi)\langle U_{1,0}\rangle - (2A/\sqrt{3})\sin^2(\theta)\langle G_{0,0}\rangle - (A/2\sqrt{6})\{2 + \cos^2(\theta)[1 + 3\cos(2\psi)]\}\langle G_{2,0}\rangle - (A/2)\{2 + \cos^2(\theta)[1 - \cos(2\psi)]\}\Re\langle G_{2,2}\rangle, \quad (3.6)$$

where $\psi = 0$, the origin of the azimuthal-angle scan, finds the c-axis of the orthorhombic crystal normal to the plane of scattering, and parallel to σ–polarization (figure 1). Multipoles with projection $Q = 0$ are purely real. Complex quantities A and B in (3.6) are fully determined by the crystal structure, while θ is the Bragg angle (figure 1). The contribution to a structure factor proportional to magnetic charge, $\langle G_{0,0}\rangle$, does not depend on the azimuthal angle, ψ, because charge is a scalar entity with $K = 0$. Dependence of $F_{\pi'\sigma}(\text{E1-M1})$ on the azimuthal angle is accomplished by a polar dipole, $\langle U_{1,0}\rangle$, and magneto-electric quadrupoles, $\langle G_{2,Q}\rangle$.

Magnetic charge does not contribute to any dichroic signal of which three, from a total of five, are parity-odd. In fact, of all the multipoles in the structure factor (3.6) for Bragg diffraction only magneto-electric quadrupoles $\langle G_{2,2}\rangle$ can be observed in a dichroic signal, specifically non-reciprocal linear dichroism. General expressions for all five dichroic signals are gathered in [23] which analyses the dichroism displayed by copper metaborate in a magnetic field.

4. Experiments

In this section we present some recent experimental results that demonstrate the sensitivity of resonant x-ray Bragg diffraction to families of atomic multipoles representing the degrees of freedom of electrons in the ground state.

4.1. UO_2

The nature of the low temperature ground state of uranium dioxide ($Fm\bar{3}m$ space group) has long been studied. Below the Néel temperature $T_\mathrm{N} = 31$ K, a complicated magnetic structure of the **3k** variety is reported. Associated with T_N is also a rearrangement of the oxygen atoms [24]. Significant theoretical work was performed to explain this rich behaviour [25–28]. All such theories emphasize the importance of interplay between Jahn–Teller and quadrupolar interactions.

However, direct measurement of quadrupolar ordering proved elusive until the advantages inherent to resonant x-ray Bragg diffraction were fully appreciated, e.g., site selectivity, enhanced signal strength, and polarization analysis. An elegant experiment by Wilkins *et al* [29] on UO_2 provided direct experimental evidence of ordering of the quadrupoles associated with the uranium ions. By using resonant x-ray diffraction, enhanced by the uranium M_4-edge, Wilkins *et al* [29] were able to measure directly the presence of quadrupolar ordering. Exploitation of polarization analysis on the secondary beam together with azimuthal-angle scans (rotation of the sample about the Bragg wavevector) enabled the separation of the magnetic and the non-magnetic quadrupole contribution in the total intensity.

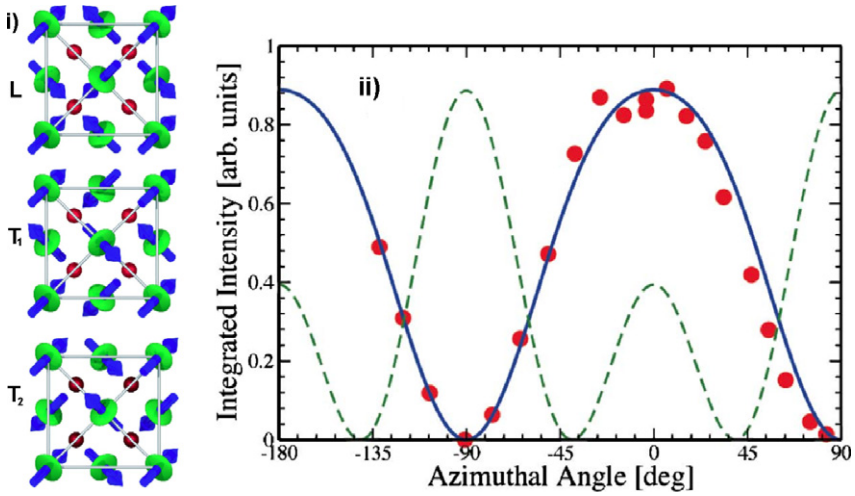

Figure 2. (i) Schematic representation of the projection onto the a–b plane of the 3**k** magnetic and electric quadrupole ordering for the longitudinal (L) and the two transverse configuration (T_1 and T_2). Magnetic moments are represented by arrows whereas the electric quadrupole moments are shown as ellipsoids; (ii) integrated intensity as a function of the azimuthal angle for the (1, 1, 2) reflection measured in the σ'–σ channel (circles). The solid (dashed) line shows the expected azimuthal-angle dependence for the transverse (longitudinal) model described in [29] from which the figure is reproduced.

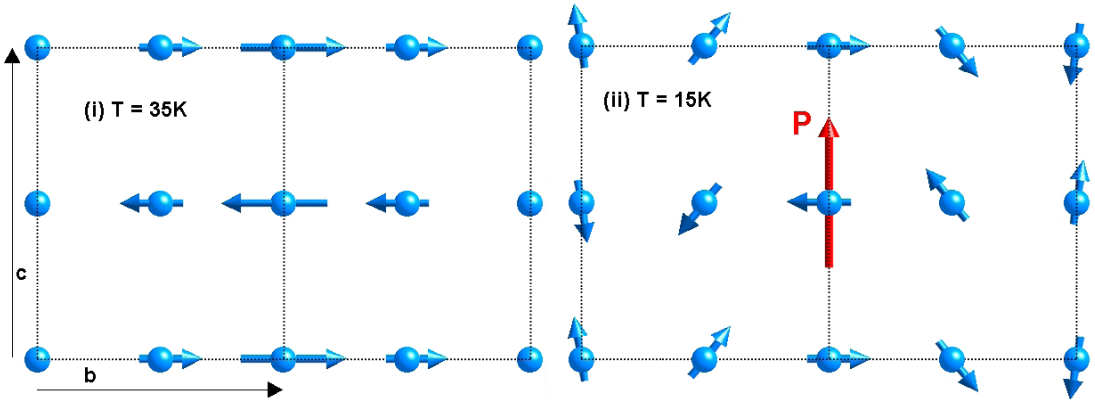

Figure 3. Magnetic ordering on the Mn sublattice in phase (i) $T = 35$ K and phase (ii) $T = 15$ K of terbium manganate as suggested by neutron scattering [30]. In phase (ii) a spiral phase violates parity (inversion symmetry) allowing an electric polarization, represented by an arrow along **c**.

In the rotated channel, σ'–π, both magnetic and quadrupole contributions are present, but the magnetic one overwhelms the quadrupolar one. Contrary to this observation, in the unrotated channel, σ'–σ, no magnetic contribution is present [6, 16] and therefore the measured resonant intensity can be ascribed entirely to quadrupole ordering. Through the study of its azimuthal-angle dependence, it is found that diffracted intensity can be explained as an incoherent sum of two transverse domains (figure 2). The azimuthal-angle dependence also rules against Thomson (charge) scattering, as it is not expected to show any azimuthal dependence. In this example of resonant Bragg diffraction, the technique provided key evidence in favour of quadrupolar ordering with the directness peculiar only to it.

4.2. $TbMnO_3$

$TbMnO_3$ has recently attracted much attention because of its multiferroic properties [12]. In an interval of temperature 28 K $< T <$ 41 K, which we call phase (i), magnetization exists on the Mn sublattice which is collinear, polarized along **b**, and incommensurate with a wave vector $\mathbf{q} \sim 0.28\mathbf{b}^*$ (figure 3(i)), while Tb ions are not magnetically ordered. Long-range magnetic order is accompanied by a modulation of the Mn sublattice with sinusoidal displacements along **c**. Within the temperature range 7 K $< T <$ 28 K, called phase (ii), modifications create a multiferroic state. A spatially varying electric dipole moment, associated with Mn displacements, undergoes a first-order transition to a ferroelectric phase that contributes spontaneous polarization along **c** (figure 3(ii)). Simultaneously, magnetization on the Mn sublattice becomes non-collinear with a component along **c**. Terbium magnetic moments in phase (ii) display non-collinear order, with transverse polarization along **a** and wave vector **q**.

Observation of a magnetically controlled ferroelectric polarization in terbium manganate demonstrates a giant magneto-electric effect [9]. Below 7 K, labelled phase (iii), Tb moments adopt the same configuration as in phase (ii) but

the wave vector is distinctly different, namely, $\mathbf{q}' \sim 0.42\mathbf{b}^*$. Here we concentrate on recent resonant x-ray Bragg diffraction studies [31, 32].

In an effort to understand modifications to terbium manganate occurring in the different phases, many azimuthal-angle scans as well as energy dependence at the Mn K- and Tb L_3-edges were collected. Let us recall major findings. In phase (i) Mannix *et al* [32] found A-type $(0, 4 \pm q, 1)$ and F-type $(0, 4 \pm q, 0)$ reflections at the Mn K- and Tb L_3-edges, and only A-type reflections with a primary photon energy far from absorption edges. Presence of diffracted intensity at the Tb L_3-edges is attributed to Tb 5d-state polarization induced by ordering of Mn magnetic moments.

The development of a non-collinear Mn substructure in phase (ii) removes inversion symmetry. An E1–E2 scattering channel is then allowed in resonant x-ray Bragg diffraction. Indeed, pronounced differences in energy spectra collected at the Mn K- and Tb L_3-edges are clearly visible (figures 10, 13 and 14 in [32]). A new set of satellite reflections $(0, 3 \pm q, 0)$, associated with non-collinear ordering (C-type), was observed at the Tb L_3-edge but not at the Mn K-edge. These experimental observations have been successfully analysed by Scagnoli and Lovesey [15] using the formalism described here in equations (3.3) and (3.4). This method of attack on the data does not rely on knowledge of the space group symmetry of the low temperature phases of $TbMnO_3$, which is not precisely known. Figure 4 shows a calculated azimuthal-angle dependence of the C-type reflection $(0, 3 + q, 0)$ in the rotated channel of polarization in the vicinity of the Tb L_3-edge. Good agreement between calculated and observed intensities is evident. Scagnoli and Lovesey [15] show that the low temperature satellite reflections originate from dipole–dipole (E1–E1) and dipole–quadrupole (E1–E2) events, while the quadrupole–quadrupole (E2–E2) event can be excluded. Presence of the E1–E2 event in diffraction suggests an intricate coupling between charge and magnetic degrees of freedom in terbium manganate.

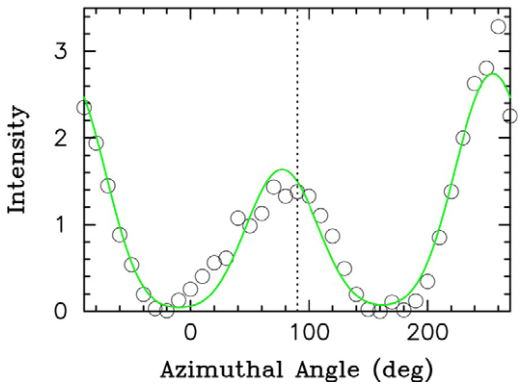

Figure 4. Data collected in the π'–σ channel at a C-type reflection $(0, 3 + q, 0)$ in phase (ii) are reproduced from figure 20 in Mannix *et al* [32]. Data were gathered with a primary energy corresponding to the E1–E1 event around 7.520 keV in the vicinity of the Tb L_3-edge. Solid curve is a fit to intensity proportional to the expression $(t - \cos\psi + d\cos 2\psi + u\sin\psi + w\sin 2\psi)^2$ developed by Scagnoli and Lovesey [15] who provide the physical origin in terms of atomic multipoles of the various parameters. The origin of the azimuthal angle, ψ, is denoted by a vertical line, displaced by 90° from the origin used by Mannix *et al* [32].

4.3. Right- or left-handed?

Enantiomers, or stereoisomers, have crystal structures that are mirror images of each other and are thus handed, like our right and left hands. Physical properties of enantiomers are identical except for optical activity, which rotates linearly polarized light by equal amounts but in opposite directions. While conventional x-ray Bragg diffraction can determine crystal structures, it does not distinguish right- and left-handed crystals. However, resonant x-ray diffraction, using circularly polarized x-rays, can reveal the handedness of crystals through a coupling of x-ray helicity with the enantiomorphic screw-axis.

Sensitivity of resonant x-ray Bragg diffraction to the handedness of crystals is readily inferred by examination of the scattered intensity. We describe x-ray polarization by Stokes parameters P_2 and P_3 [6, 7] and with full polarization $(P_2)^2 + (P_3)^2 = 1$. The parameter P_2 is the mean helicity in the beam, and P_3 is the linear polarization with $P_3 = +1(-1)$ corresponding to complete linear σ-polarization normal (π-polarization parallel) to the plane of scattering (figure 1).

With this notation, the total intensity from a primary beam endowed only with circularly polarization ($P_1 = P_3 = 0$) is,

$$I_0 = P_2\,\mathrm{Im}\{(G_{\sigma'\pi})^*(G_{\sigma'\sigma}) + (G_{\pi'\pi})^*(G_{\pi'\sigma})\} + 1/2\{|G_{\sigma'\pi}|^2 + |G_{\sigma'\sigma}|^2 + |G_{\pi'\pi}|^2 + |G_{\pi'\sigma}|^2\}, \qquad (4.1)$$

where an amplitude $G_{\mu'\nu}$ is defined in (2.1), and * denotes complex conjugation. For Thomson scattering the coefficient of P_2 is identically zero, because there are no contributions to diffraction in channels with rotated polarization, σ'–π and π'–σ. However, the coefficient can be different from zero for resonant diffraction since all four channels of scattering may be different from zero. Such is the case when the crystal contains an enantiomorphic screw-axis. Thanks to the specificity of resonant Bragg diffraction, Tanaka *et al* were able to reveal the handedness of quartz enantiomers [33].

Quartz illustrated in figure 5 uses sites with multiplicity 3 and Wyckoff letter a for silicon ions in $P3_121$ (#152, right-handed, R in the following) and $P3_221$ (#154, left-handed, L in the following). It is possible to show [21] for the reflection $(0, 0, l)$ that structure factors $\mathbf{\Psi}^K$ (equation (3.2)) of the enantiomorphic space-group pair obey the identity,

$$\mathbf{\Psi}^K_Q(\#154) = (-1)^K \mathbf{\Psi}^K_{-Q}(\#152), \qquad (4.2)$$

that in turn leads to structure factors which satisfy,

$$F_{\mu'\nu}(\#152, \psi) = \pm\{F_{\mu'\nu}(\#154, \psi)\}^*, \qquad (4.3)$$

with the plus (minus) for a parity-even (odd) event. If we look back at equation (4.1) for the total intensity I_0, it follows from (4.3) that the coefficient of P_2 is of opposite sign for the enantiomers (the reader is advised to consult [21] for the complete $F_{\mu'\nu}$). In other words, in diffraction enhanced by a single resonant event, circular polarization (x-ray helicity) and crystal chirality are directly coupled. Sign differences in (4.3) are a simple and direct consequence of differences

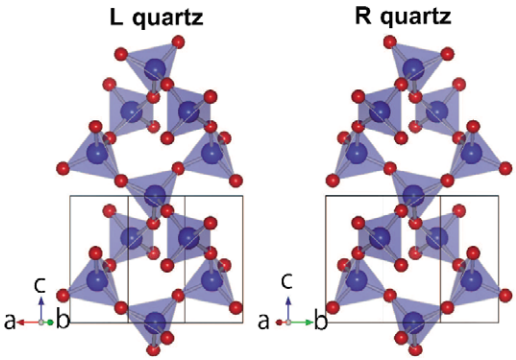

Figure 5. Views of atomic structure in R quartz (right) and L quartz (left) along the **a** axis and the **b** axis, respectively. The **a** and **b** axes are normal to the plane of paper. Large and small spheres represent Si and O atoms, respectively. Lines show the unit cell with hexagonal axes. Reproduced from [33]. Copyright 2008 by the American Physical Society.

between $\mathbf{J}^{K}_{\mu'\nu}$ (which describes the condition of the primary and secondary photons in equation (3.1)) for the two types of resonant event considered.

Figure 6 shows integrated intensity at the reflection $(0, 0, 1)$ as a function of azimuthal angle, ψ, from R and L forms of quartz. A sinusoidal modulation exhibiting threefold periodicity of the enantiomorphic screw-axis is observed. Integrated intensity for R quartz for incident left circular polarization (LCP) and that of L quartz for right circular polarization (RCP) are comparable, and there is a pronounced intensity modulation on sweeping the azimuthal angle. By inverting the primary polarization, respectively for the two crystals, the integrated intensities are still comparable with each other, while the intensity modulation has almost disappeared. The presence of this asymmetry is attributed by Tanaka *et al* [33] to an admixture of E1–E1 and E1–E2 events. If only one event contributed to diffraction, intensities for LCP and RCP for a given form of quartz would exhibit an antiphase relation with each other, with the same intensity variation as a function of the azimuthal angle. Similar arguments would apply if we consider L and R quartz with the same primary circular light.

While helicity of x-rays cannot couple to Thomson scattering, because it is diagonal with respect to photon polarization, helicity may couple to chirality in the configuration of magnetic moments. We consider scattering from pure spin moments whose spatial Fourier transform is $\mathbf{S}(\mathbf{k}) = \Sigma \mathbf{S}_j \exp(\mathrm{i}\mathbf{k}\cdot\mathbf{R}_j)$ with $\mathbf{k} = \mathbf{q} - \mathbf{q}'$ and $\mathbf{k}$ anti-parallel to the x-axis, as depicted in figure 1. The coefficient of P_2 in the cross-section for total scattering is proportional to a component of the static correlation function made from a vector product of $\mathbf{S}(\mathbf{k})$ and its Hermitian conjugate, namely, the x-component of $\langle \mathbf{S}(-\mathbf{k}) \times \mathbf{S}(\mathbf{k})\rangle$ where $\mathbf{S}(-\mathbf{k})$ is the Hermitian conjugate of $\mathbf{S}(\mathbf{k})$. The fact that this time-even correlation function appears in the cross-section multiplied by x-ray helicity is proof that it is a chiral order parameter. From expression (8.93) in [16] for the partial differential cross-section one finds a total cross-section for scattering from spins,

$$\mathrm{d}\sigma/\mathrm{d}\Omega = \mathrm{i}4(r_\mathrm{e}E/mc^2)^2\cos^2(\theta)\sin^3(\theta)P_2 \times \langle \boldsymbol{\eta}\cdot\{\mathbf{S}(-\mathbf{k}) \times \mathbf{S}(\mathbf{k})\}\rangle, \quad (4.4)$$

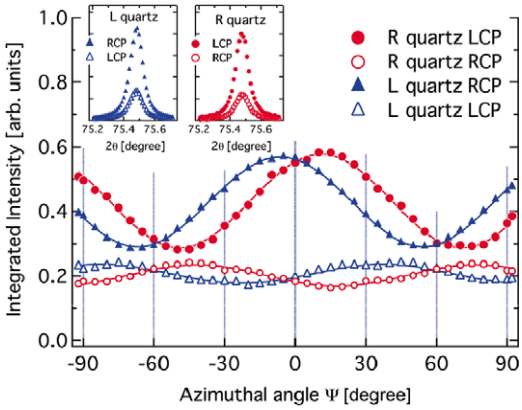

Figure 6. Shown are integrated intensities of the reflection $(0, 0, 1)$ of R and L quartz as a function of azimuth angle ψ. Filled (open) circles represent the intensity of R quartz measured with LCP (RCP) primary beam, and filled (open) triangles represent the intensity of L quartz measured with RCP (LCP) primary beam. Each continuous line is a fit to data. Insets show 2θ-scan profiles of the reflection $(0, 0, 1)$ observed with $\psi = 0°$. Reproduced from [33]. Copyright 2008 by the American Physical Society.

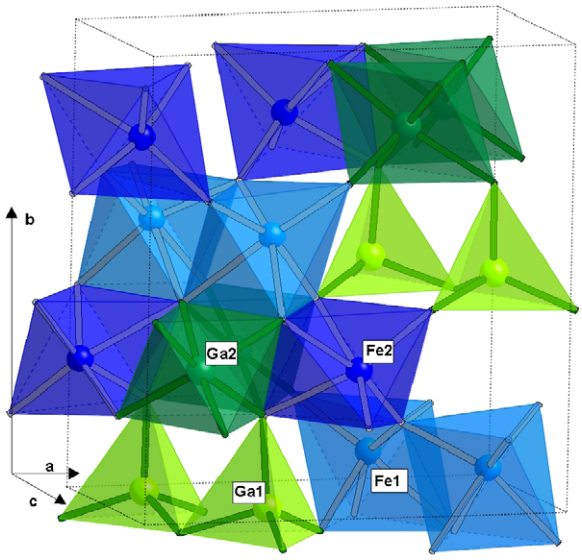

Figure 7. The crystal structure (space group $Pc2_1n$) of gallium ferrate ($GaFeO_3$).

where the unit vector $\boldsymbol{\eta} = \mathbf{k}/k$, $r_\mathrm{e} = 0.282 \times 10^{-12}$ cm is the classical radius of the electron and E is the x-ray energy. In (4.4), 2θ is the angle through which x-rays are deflected. The trigonometric function $\cos^2(\theta)\sin^3(\theta)$ vanishes at the extremes, $\theta = 0°$ and $90°$, and has its maximum when $2\theta = 101.54°$ at which it achieves a value $= 0.19$.

4.4. $GaFeO_3$

At room temperature, the orthorhombic structure (space group $Pc2_1n$) of gallium ferrate ($GaFeO_3$) belongs to the C_{2v} polar crystal class [34, 35] with spontaneous electric polarization along the **b** axis (figure 7). Sites in this structure occupied by Fe ions ($3d^5$) have no symmetry. Below a temperature $\approx$200 K, collinear ferrimagnetism [36] and the magneto-

electric effect [12, 37] develop, with the magnetic easy-axis along the crystal **c** axis.

Results for gallium ferrate derived from dichroic signals, gathered in the optical [38] and x-ray [39] regions of energy, and x-ray Bragg diffraction enhanced by the iron K-edge resonance [40] appeared recently. Here, we focus our attention on results derived from resonant Bragg diffraction. With the use of an ac magnetic field (strength 50 mT and frequency 10 Hz) applied along the magnetization easy-axis, Arima *et al* [40] took advantage of interference properties intrinsic in resonant diffraction.

The diffracted intensity $I_1(I_2)$ for a given Bragg reflection was measured for magnetic field orientation parallel (anti-parallel) to the magnetization easy-axis, and the intensity difference $\Delta I = I_1 - I_2$ was then considered. The advantage of considering the intensity difference, ΔI, is that time-even quantities (whose sign does not change with reversal of the polarity of the applied magnetic field) cancel out, leaving an intensity strongly depending on the (usually) weak magneto-electric contributions (E1–E2 and E1–M1). Arima *et al* [40] invoke the presence of toroidal moments (represented here by the anapole $\langle \mathbf{G}_1 \rangle$ in table 1) associated with an E1–E2 event to explain the observed data. Subsequent *ab initio* calculations by Di Matteo and Joly [41] underlined the possible presence of octupoles as well as magnetic quadrupoles. However, their simulation does not represent the experimental results at all well.

Lovesey *et al* [22] overcame all the apparent difficulties and interpreted the data successfully. Introduction in the scattering amplitude (following the method outlined in sections 2 and 3) of an additional term responsible for E1–M1 scattering was vital to reproduce the experimental results. Figure 8 illustrates the good agreement between the calculated energy dependence and the experimental data of all specular reflections measured. Lovesey *et al* [22] also explain the dichroic signals at the Mn K-edge [39] and in the optical region [38]. It is important to stress once more that the presence of such contributions is possible because $GaFeO_3$ possesses a non-centrosymmetric crystal structure and sites occupied by Fe ions have no symmetry.

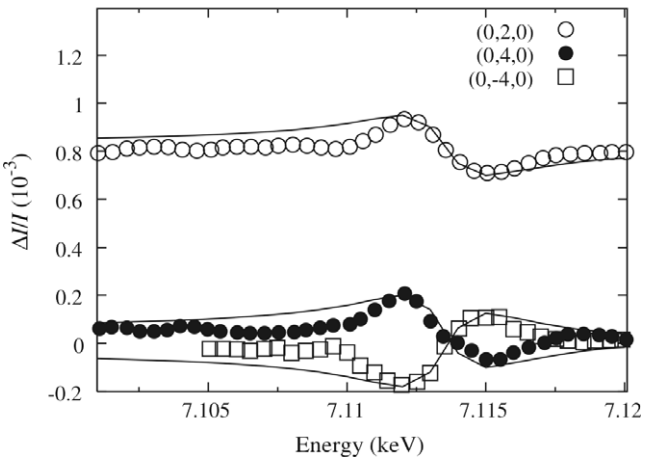

Figure 8. Experimental data on a field difference of intensities $\Delta I/I$ from gallium ferrate. Sample temperature 50 K, and data are for reflections $(0, k, 0)$ with Miller indices $k = 2, 4$ and -4. Continuous curves are fits to a theoretical simulation developed by Lovesey *et al* [22].

5. Discussion

We reviewed some recent experimental findings derived from resonant x-ray Bragg diffraction. It is a versatile technique that can be applied to different materials, ranging from antiferromagnetic to multiferroic systems. Taking advantage of element and site specificity, polarization analysis and azimuthal-angle scans, resonant x-ray Bragg diffraction proves itself an ideal tool to investigate subtle and enigmatic ordering of charge and magnetic phenomena. As every powerful tool, it has its drawbacks, and usually experiments prove extremely difficult to perform. In this respect, neutron Bragg diffraction is a handier tool to determine both the configuration and distribution of magnetization in a crystal [42]. However, when considering physical effects originating from subtle changes to the structure of materials (electronic and crystallographic), resonant x-ray diffraction is second to none.

Small changes in electric and magnetic degrees of freedom cannot be easily detected with ordinary techniques, such as x-ray high-resolution powder diffraction. An example is $TbMnO_3$ whose orthorhombic *Pbnm* structure proves incompatible with the multiferroic effects observed on the Mn site. In this space group, sites occupied by Mn ions possess an inversion symmetry that does not allow admixture of orbitals of different parity, a key ingredient to multiferroicity. With resonant x-ray diffraction such symmetry breaking effects are relatively easy to detect.

Understanding magneto-electric and allied effects in complex materials brings to play composite atomic variables constructed from charge and magnetic electron degrees-of-freedom. The role of these quantities, readily calculable as outlined in sections 2 and 3, are of fundamental importance in understanding electronic phenomena at the atomic level. In order to better identify which particular multipole (see section 3) is contributing to a given extent to the scattering amplitude, experiments in the soft x-ray regime might have an important role to play. As an example, observation of the forbidden $(0, k, 0)$ reflection with Miller index $k = 1$ from multiferroic gallium ferrate ($GaFeO_3$), enhanced by Fe absorption L-edges at ≈710 eV, might give decisive information on multipoles contributing to the E1–M1 scattering amplitude (3.6). Notably, predicted strange atomic multipoles that are both time-odd and parity-odd (table 1), include a magnetic charge, $\langle \mathbf{G}_0 \rangle$, and a magnetic quadrupole, $\langle \mathbf{G}_2 \rangle$.

Acknowledgments

We are grateful for discussion and correspondence with E Balcar, S P Collins, J M Hancock, K S Knight, U Staub, Y Tanaka and S Wilkins.

Appendix A

Contributions to resonant x-ray diffraction enhanced by the E1–M1 event are explored with a model wavefunction for

the equilibrium, ground state of a resonant ion. The wave function chosen for this exercise is an admixture of p-like and d-like single-particle, atomic states. Mixing parameters may originate from several sources, including, odd-order contributions to the crystal electric field, configuration interaction and covalency. There are two d-states, with angular symmetry yz plus z^2, chosen so that a parity-even quadrupole that may appear in the E1–E1 structure factor is different from zero while the orbital angular momentum is zero. (The parity-even quadrupole contributes Templeton and Templeton scattering [1, 3, 5].) For a p-state we choose $|l', 0\rangle$ with angular momentum $l' = 1$ which has z-like angular symmetry and no orbital angular momentum because the projection $= 0$. Mixture of the states $|l, 0\rangle$ and $|l', m\rangle$ with $l = 2$ and $l' = 1$ in the wavefunction allow parity-odd multipoles to be different from zero. Electron spin is saturated with a wavefunction $|s = 1/2, m_s = 1/2\rangle$.

The complete wavefunction for the resonant ion is product state,

$$\aleph^{1/2}|s = 1/2, m_s = 1/2\rangle\{|l, 0\rangle + \mathrm{i}b(|l, +1\rangle + |l, -1\rangle)/\sqrt{2} + f|l', 0\rangle\}, \tag{A.1}$$

with the normalization $\aleph$ determined by $\aleph(1 + b^2 + |f|^2) = 1$. In (A.1), the parameter f is allowed to be a complex number, $f = f' + if''$, and it measures mixing of the two states with opposite parity.

To learn more about the model wavefunction we consider expectation values of cameo monopoles and dipoles listed in table 1. The parameter b in (A.1) is chosen to be purely real and consequently expectation values of the orbital angular momentum are zero, i.e., $\langle L_\beta\rangle = 0$ for $\beta = x$, y or z leading to $\langle\mu_\beta\rangle = 0$ for $\beta = x$ or y and $\langle\mu_z\rangle = 1$.

Next, consider expectation values of parity-odd operators related to the mixing parameter f. Let us start with polar multipoles. One finds the model state possesses chirality proportional to the imaginary part of f,

$$\langle\boldsymbol{\mu}\cdot\boldsymbol{\Omega}\rangle = -8\aleph f''/\sqrt{15}, \tag{A.2}$$

while polar dipoles $\langle\mathbf{U}_1\rangle = \langle\mathbf{R}\rangle$ that do not vanish are proportional to the real part of f, namely,

$$\langle R_x\rangle = 0, \langle R_y\rangle = 2\aleph bf'/\sqrt{5}, \langle R_z\rangle \equiv \langle R_0\rangle = 4\aleph f'/\sqrt{15}. \tag{A.3}$$

Note that $\langle R_y\rangle = 0$ if $b = 0$, and in this limit chirality and the displacement $\langle R_z\rangle$ can be different from zero. Turning to magneto-electric multipoles, we learn that (A.1) possesses magnetic charge if the real part of f is different from zero. The result,

$$\langle\boldsymbol{\mu}\cdot\mathbf{R}\rangle = 4\aleph f'/\sqrt{15}, \tag{A.4}$$

can actually be deduced from (A.2) using a relation given with table 1 between equivalent operators representing chirality and magnetic charge. Components of the anapole possessed by the state (A.1) are,

$$\langle\Omega_x\rangle = -4\aleph bf'/\sqrt{5}, \qquad \langle\Omega_y\rangle = -8\aleph bf''/\sqrt{5}, \qquad \langle\Omega_z\rangle = -16\aleph f''/\sqrt{15}. \tag{A.5}$$

Results (A.2)–(A.5) illustrate correlations that can exist between polar and magneto-electric multipoles.

Operators in table 1 are cameo operator equivalents for atomic quantities of interest in understanding electron degrees of freedom in scattering and dichroic signals that engage a parity-odd event. To construct operators that generate quantities actually observed one must work with the appropriate scattering amplitude, which is a complicated animal [6, 7]. The dependence of a unit-cell structure factor on the total angular momentum of the intermediate state, J_c, is the same for both parity-even and parity-odd events. Proof of this statement for parity-odd structure factors is non-trivial for it uses new identities for $12j$ Racah symbols [45, 46]. The very simple dependence of structure factors on J_c yields the celebrated sum rules derived by Thole and collaborators for dichroic signals created by parity-even events [43, 44].

Observed multipoles are defined by reference to the scattering amplitude. Let $\Upsilon_{K,Q}$ denote the electron operator appearing in the parity-odd amplitude [6, 7, 46]. The relation to our polar and magneto-electric operators is,

$$\Upsilon_{K,Q} = \mathrm{i}^{K-1}U_{K,Q} - \mathrm{i}^K G_{K,Q}. \tag{A.6}$$

Unlike $\Upsilon_{K,Q}$, polar and magneto-electric operators possess, by design, definite parity and definite time-reversal signatures. Using our model wavefunction (A.1), the polar multipole in the E1–M1 structure factor (3.6) is,

$$\langle U_{1,0}\rangle = 0 : \mathrm{L}_2 \text{ edge}, \qquad \langle U_{1,0}\rangle = \sqrt{(1/30)}\aleph f' : \mathrm{L}_3 \text{ edge}. \tag{A.7}$$

Notable is the null value of $\langle U_{1,0}\rangle$ at the L_2-edge, whereas $\langle U_{1,0}\rangle$ at the L_3-edge and $\langle R_0\rangle$ in (A.3) may be different from zero.

Magnetic charge that can be observed in the state (A.1) is found to be,

$$\langle G_{0,0}\rangle = (1/9)\sqrt{(1/5)}\aleph f' : \mathrm{L}_2 \text{ edge}, \qquad \langle G_{0,0}\rangle = (2/9)\sqrt{(1/5)}\aleph f' : \mathrm{L}_3 \text{ edge}. \tag{A.8}$$

It can be shown that, the contribution to a structure factor from a monopole is proportional to $(2J_c + 1)$ [46]. This result is illustrated in (A.8) by values for $\langle G_{0,0}\rangle$ at the L_2-edge ($J_c = 1/2$) and the L_3-edge ($J_c = 3/2$). Thus a more fundamental statement is that the monopole contribution to a polar structure factor is proportional to $\{(2J_c + 1)\langle\boldsymbol{\mu}\cdot\Omega\rangle\}$, and the corresponding contribution to a magneto-electric structure factor is proportional to $\{(2J_c+1)\langle\boldsymbol{\mu}\cdot\mathbf{R}\rangle\}$. For magneto-electric quadrupoles we find,

$$\langle G_{2,0}\rangle = (1/9)\sqrt{(2/5)}\aleph f' : \mathrm{L}_2 \text{ edge}, \qquad \langle G_{2,0}\rangle = (2/5)\sqrt{(2/5)}\aleph f' : \mathrm{L}_3 \text{ edge}, \tag{A.9}$$

where the dependence on J_c is different from that found for a monopole. The multipole $\langle G_{2,2}\rangle$ is zero at both edges because (A.1) does not permit $Q = \pm 2$.

Appendix B

E1–M1 unit-cell structure factors listed here are calculated from (3.4) and (3.5) using the Wigner rotation matrix $D^K_{Q,q}(\psi) = \exp\{i\pi(Q-q)/2\}d^K_{Q,q}(\psi)$, and x-ray factors listed in table 2. Expressions given here have been cross-checked with two independent calculations. The one significant difference between E1–M1 and E1–E2 unit-cell structure factors is that $F_{\pi'\sigma}$ (E1–M1) is a function of $\mathbf{A}_{K,Q}$ while $F_{\pi'\sigma}$(E1–E2) is a function of both $\mathbf{A}_{K,Q}$ and $\mathbf{B}_{K,Q}$.

Polar; $\langle U_{K,Q}\rangle$

$$F_{\sigma'\sigma} = \sin(\theta)[-2iB_{1,1} + i\sqrt{(3/2)}\sin(2\psi)A_{2,0} - 2\cos(2\psi)A_{2,1} + i\sin(2\psi)A_{2,2}].$$

$$F_{\pi'\sigma} = (2i/\sqrt{3})\cos^2(\theta)A_{0,0} - (i/\sqrt{2})\sin(2\theta)\cos(\psi)A_{1,0} - \sin(2\theta)\sin(\psi)A_{1,1} + i/(2\sqrt{6})[3(1+\sin^2(\theta))\cos(2\psi) - \cos^2(\theta)]A_{2,0} + (1+\sin^2(\theta))\sin(2\psi)A_{2,1} + (i/2) \times [(1+\sin^2(\theta))\cos(2\psi) + \cos^2(\theta)]A_{2,2}.$$

$$F_{\sigma'\pi}(\theta) = -F_{\pi'\sigma}(-\theta).$$

$$F_{\pi'\pi} = \sin(\theta)[2iB_{1,1} + i\sqrt{(3/2)}\sin(2\psi)A_{2,0} - 2\cos(2\psi)A_{2,1} + i\sin(2\psi)A_{2,2}].$$

Note (a) $F_{\sigma'\sigma}$ and $F_{\pi'\pi}$ are the same apart from the sign of $B_{1,1}$ (b) $F_{\sigma'\pi}$ and $F_{\pi'\sigma}$ are composed of $A_{K,Q}$ and not $B_{K,Q}$. Moreover, these unit-cell structure factors are the same apart from signs attached to the pseudo-tensors, i.e., in the two channels with rotated polarization chiral quantities have opposite signs.

Magneto-electric; $\langle G_{K,Q}\rangle$

$$F_{\sigma'\sigma} = \cos(\theta)[-\sqrt{2}\sin(\psi)A_{1,0} - 2i\cos(\psi)A_{1,1} - 2\cos(\psi)B_{2,1} + 2i\sin(\psi)B_{2,2}].$$

$$F_{\pi'\sigma} = -(2/\sqrt{3})\sin^2(\theta)A_{0,0} - (1/\sqrt{2})\sin(2\theta)\cos(\psi)A_{1,0} + i\sin(2\theta)\sin(\psi)A_{1,1} - 1/(2\sqrt{6}) \times [2+\cos^2(\theta)(1+3\cos(2\psi))]A_{2,0} + i\cos^2(\theta)\sin(2\psi)A_{2,1} + (1/2) \times [2+\cos^2(\theta)(1-\cos(2\psi))]A_{2,2}.$$

$$F_{\sigma'\pi}(\theta) = F_{\pi'\sigma}(-\theta).$$

$$F_{\pi'\pi} = \cos(\theta)[-\sqrt{2}\sin(\psi)A_{1,0} - 2i\cos(\psi)A_{1,1} + 2\cos(\psi)B_{2,1} - 2i\sin(\psi)B_{2,2}].$$

Note (a) $F_{\sigma'\sigma}$ and $F_{\pi'\pi}$ are the same apart from the signs of $B_{K,Q}$ and (b) $F_{\sigma'\pi}$ and $F_{\pi'\sigma}$ are composed of $A_{K,Q}$ and not $B_{K,Q}$. Moreover, these structure factors are the same apart from signs attached to the true-tensors. Thus in the two channels with rotated polarization magnetic charge, $A_{0,0}$, is the same.

Appendix C

Parity; one discrete symmetry of a variable is its behaviour with respect to inversion of spatial coordinates, when Cartesian components $x, y, z \to -x, -y, -z$. A variable is parity-even (parity-odd) if it is unchanged (changes sign) by inversion. The position variable, $\mathbf{R} = (x, y, z)$, is a polar vector (dipole) and parity-odd. Spin and orbital angular momentum are parity-even, i.e., these dipole variables behave as axial vectors. The product of charge conjugation (by which we mean particle–antiparticle conjugation), parity, and time-reversal is denoted by CPT. Because of relativistic invariance, the CPT transformation always commutes with the Hamiltonian. For the C and P (and therefore T) transformations separately, experiment shows that the electromagnetic interactions are invariant.

Time-reversal; time-reversal applied to momentum or electron spin changes the sign, and variables with this property are called time-odd. Time-even variables do not change sign under time-reversal, e.g., the position of an electron. The spin, $\mathbf{S}$, satisfies the commutation relation $\mathbf{S} \times \mathbf{S} = i\mathbf{S}$, with $i = \sqrt{(-1)}$. Thus ($i\mathbf{S}$) is time-even because it is a (vector) product of identical operators possessed of a definite time-reversal signature, namely, odd. A magnetic field (electric field) is time-odd (time-even). Zeeman and electric dipole interactions are unchanged by time-reversal for each interaction is a product of two variables that behave in the same way under time-reversal.

Helicity and chirality; a variable or material that has right-handed or left-handed quality, which is not superposable on its mirror image, is said to possess helicity or chirality. Helicity is a parity-odd and time-even property. The helicity of light is often quoted in terms of a Stokes parameter that is a purely real, pseudo-scalar and time-even quantity. A magnetic field is not handed, and a magnetic field by or in itself does not resolve an achiral (racemic) mixture.

Rank of a tensor (multipole), K; the integer $K = 0, 1, \ldots,$ etc is the rank of a tensor, or multipole. The size of the family of multipoles available in a resonant scattering event is governed by the rank of the absorption events engaged in scattering; values of K allowed in a family are given by the sum of the ranks of the events and this sum follows the triangle rule for addition of angular momentum in quantum mechanics. E.g., E1 is a (electric) dipole and corresponds to $K = 1$, and the E1–E1 event is a sum of two dipoles that generate a family of multipoles with rank $K = 0$, 1 and 2. The same result holds for E1–M1 because E1 and M1 are both dipoles. The operator for E2 is a quadrupole ($K = 2$) and the family of multipoles engaged by an E1–E2 event comprises a dipole, quadrupole and an octupole ($K = 3$).

Polar multipole $\langle \mathbf{U}_K \rangle$; this atomic multipole is constructed such that it is time-even and parity-odd for all K (rank of a multipole). The dipole $\langle \mathbf{U}_1 \rangle$ thus has properties with respect to inversion and time-reversal that match properties of the position vector, $\mathbf{R}$. The polar multipole with $K = 0$ is a scalar quantity that by construction is both parity-odd and time-even, i.e., a time-even, pseudo-scalar. $\langle \mathbf{U}_0 \rangle$ can be different from zero for electron structure that is chiral, and it is zero for an achiral structure. Thus $\langle \mathbf{U}_0 \rangle$ has properties with respect to inversion and time-reversal that match helicity, or chirality. The sum of $\langle \mathbf{U}_0 \rangle$ for every ion in the unit cell of a crystal, which is a unit-cell structure factor, can be different from zero if the crystal belongs to one of the 11 enantiomorphic crystal classes, and it is zero for all other 21 crystal classes.

Maxwell's equations; there is a strong symmetry between electric field and magnetic field, yet a magnetic charge analogous to electric charge is peculiarly absent from

Maxwell's equations [13, 14]. The source of a magnetic field is either a moving electric charge or a static magnetic dipole, never a static magnetic charge it would seem. If Maxwell's equations are symmetrized by the introduction of magnetic charge, this charge must be such that it is reversed by each of the discrete symmetries in CPT.

Magneto-electric multipole $\langle \mathbf{G}_K \rangle$; this atomic multipole is constructed such that it is time-odd and parity-odd for all K. The magneto-electric dipole has properties that match properties of an anapole, e.g., spin anapole $= \mathbf{S} \times \mathbf{R} = -\mathbf{R} \times \mathbf{S}$ where $\mathbf{S}$ is spin. Related to the anapole is the magneto-chiral effect under consideration as a mechanism for the homo-chirality of life [49]. The magneto-electric multipole with $K = 0$ is a scalar, or charge, that is both parity-odd and time-odd, symmetry properties it has in common with magnetic charge [13].

Scattering, dichroism and birefringence; scattering and absorption (dichroism) are two sides of one coin because both are directly related to the scattering amplitude. The absorption coefficient is proportional to the total cross-section for scattering. A fundamental identity, called the optical theorem, relates the total cross-section in question and the imaginary part of the scattering amplitude evaluated for forward scattering, in which the beam of light is not deflected by the sample. Very often dichroic signals are expressed as the imaginary part of the refractive index. Birefringence can be likened to the other half of dichroism being related to the real part of the refractive index and the two signals, dichroism and birefringence, are mathematically related by a Kramers–Kronig transform. Dichroism and birefringence are bulk properties of a material. Thus signals are confined by elements of symmetry found in the point group of a crystal, and there are 32 non-magnetic point groups (crystal classes). The cross-section for scattering in to an element of solid angle subtended by the sample is proportional to square of the absolute value of the scattering amplitude. Bragg diffraction is confined by elements of symmetry in the space group. There are 230 non-magnetic space groups of which 11 are enantiomorphic space group pairs, and 65 Sohncke space groups that belong to one or other of the enantiomorphic crystal classes. A book by Cracknell [47] is recommended for symmetry properties of magnetic crystals.

Total scattering; with increasing energy of the primary x-ray beam all states of a material are sampled, energy exchange with it becomes ever more a marginal effect, and total scattering is measured. An alternative point of view is that, with high energy x-rays an instantaneous picture of the material is observed. In which case, in the partial differential cross-section it is legitimate to set the time variable in the correlation function equal to zero; see, for example, section 8.9 in [16]. The total magnetic scattering of neutrons has a cross-section analogous to (4.4) and it is $(\boldsymbol{\eta} \cdot \mathbf{P})\mathrm{i}\langle \boldsymbol{\eta} \cdot \{\mathbf{S}(-\mathbf{k}) \times \mathbf{S}(\mathbf{k})\}\rangle$ where $\mathbf{P}$ is polarization in the beam [48]. Since the variables $\mathbf{P}$ and spin have the same properties it follows that the scalar product $(\boldsymbol{\eta} \cdot \mathbf{P})$ is a time-even pseudo-scalar like photon helicity.

References

[1] Templeton D and Templeton L 1982 *Acta Crystallogr.* A **38** 62
[2] Finkelstein K D *et al* 1992 *Phys. Rev. Lett.* **69** 1612
[3] Dmitrienko V 1983 *Acta Crystallogr.* A **39** 29
[4] Carra P and Thole B T 1994 *Rev. Mod. Phys.* **66** 1509
[5] Dmitrienko V *et al* 2005 *Acta Crystallogr.* A **61** 481
[6] Lovesey S W *et al* 2005 *Phys. Rep.* **411** 233
[7] Collins S P *et al* 2007 *J. Phys.: Condens. Matter* **19** 213201
[8] Cheong S-W and Mostovoy M 2007 *Nat. Mater.* **6** 13
[9] Kimura T *et al* 2003 *Nature* **426** 55
[10] Eerenstein W F *et al* 2006 *Nature* **442** 759
[11] Smirnov A I *et al* 2009 *Phys. Rev. Lett.* **102** 037202
[12] Fiebig M 2005 *J. Phys. D: Appl. Phys.* **38** R123–52
[13] Goldhaber A S 1977 *Phys. Rev.* D **16** 1815
[14] Milton K A 2006 *Rep. Prog. Phys.* **69** 1637
[15] Scagnoli V and Lovesey S W 2009 *Phys. Rev.* B **79** 035111
[16] Lovesey S W and Collins S P 1996 *X-Ray Scattering and Absorption by Magnetic Materials* (Oxford: Clarendon)
[17] Lovesey S W 1997 *J. Phys.: Condens. Matter* **9** 7501
[18] Lovesey S W *et al* 1998 *J. Phys.: Condens. Matter* **10** 501
[19] Lovesey S W *et al* 2003 *J. Phys.: Condens. Matter* **15** 4511
[20] Mulders A M *et al* 2006 *J. Phys.: Condens. Matter* **18** 11195
[21] Lovesey S W *et al* 2008 *J. Phys.: Condens. Matter* **20** 272201
[22] Lovesey S W *et al* 2007 *J. Phys.: Condens. Matter* **19** 376205
[23] Lovesey S W and Staub U 2009 *J. Phys.: Condens. Matter* **21** 142201
[24] Faber J and Lander G H 1976 *Phys. Rev.* B **14** 1151
[25] Allen S J 1968 *Phys. Rev.* **166** 530
[26] Allen S J 1968 *Phys. Rev.* **167** 492
[27] Magnani N *et al* 2005 *Phys. Rev.* B **71** 054405
[28] Ippolito D *et al* 2005 *Phys. Rev.* B **71** 064419
[29] Wilkins S *et al* 2006 *Phys. Rev.* B **73** 060606R
[30] Kenzelmann M *et al* 2005 *Phys. Rev. Lett.* **95** 087206
[31] Voigt J *et al* 2007 *Phys. Rev.* B **76** 104431
[32] Mannix D *et al* 2007 *Phys. Rev.* B **76** 184420
[33] Tanaka Y *et al* 2008 *Phys. Rev. Lett.* **100** 145502
[34] Wood E A 1960 *Acta Crystallogr.* **13** 682
[35] Abrahams S C *et al* 1965 *J. Chem. Phys.* **42** 3957
[36] Frankel R B *et al* 1965 *Phys. Rev. Lett.* **15** 958
[37] Rado G T 1964 *Phys. Rev. Lett.* **13** 335
[38] Jung J H *et al* 2004 *Phys. Rev. Lett.* **93** 037403
[39] Kubota M *et al* 2004 *Phys. Rev. Lett.* **92** 137401
[40] Arima T *et al* 2005 *J. Phys. Soc. Japan* **74** 1419
[41] Di Matteo S and Joly Y 2006 *Phys. Rev.* B **74** 014403
[42] Brown P J 1993 *Int. J. Mod. Phys.* B **7** 3029
[43] Thole B T *et al* 1992 *Phys. Rev. Lett.* **68** 1943
[44] Carra P *et al* 1993 *Phys. Rev. Lett.* **70** 694
[45] Balcar E and Lovesey S W 2009 Tracts in modern physics *Introduction to The Graphical Theory of Angular Momentum* vol 234 (Berlin: Springer)
[46] Lovesey S W and Balcar E 2009 *J. Phys.: Condens. Matter* submitted
[47] Cracknell A P 1975 *Magnetism in Crystalline Materials* (Oxford: Pergamon)
[48] Lovesey S W and Watson G I 1998 *J. Phys.: Condens. Matter* **10** 6761
[49] Breslow R and Cheng Z-L 2009 *Proc. Natl. Acad. Sci.* **106** 9144